Neural mechanisms underlying heterogeneity in the presentation of anxious temperament

Alexander J. Shackman[a,b,c,1], Andrew S. Fox[a,b,c,d,e,f,1], Jonathan A. Oler[a,b,c], Steven E. Shelton[a,b], Richard J. Davidson[a,b,d,e,f], and Ned H. Kalin[a,b,c,d,f,2]

[a]Department of Psychiatry, [d]Department of Psychology, [c]Lane Neuroimaging Laboratory, [e]Center for Investigating Healthy Minds, [b]HealthEmotions Research Institute, and [f]Waisman Laboratory for Brain Imaging and Behavior, University of Wisconsin, Madison, WI 53719

Edited by Bruce S. McEwen, The Rockefeller University, New York, NY, and approved February 22, 2013 (received for review August 18, 2012)

Children with an anxious temperament (AT) are at risk for developing psychiatric disorders along the internalizing spectrum, including anxiety and depression. Like these disorders, AT is a multidimensional phenotype and children with extreme anxiety show varying mixtures of physiological, behavioral, and other symptoms. Using a well-validated juvenile monkey model of AT, we addressed the degree to which this phenotypic heterogeneity reflects fundamental differences or similarities in the underlying neurobiology. The rhesus macaque is optimal for studying AT because children and young monkeys express the anxious phenotype in similar ways and have similar neurobiology. Fluorodeoxyglucose (FDG)-positron emission tomography (FDG-PET) in 238 freely behaving monkeys identified brain regions where metabolism predicted variation in three dimensions of the AT phenotype: hypothalamic-pituitary-adrenal (HPA) activity, freezing behavior, and expressive vocalizations. We distinguished brain regions that predicted all three dimensions of the phenotype from those that selectively predicted a single dimension. Elevated activity in the central nucleus of the amygdala and the anterior hippocampus was consistently found across individuals with different presentations of AT. In contrast, elevated activity in the lateral anterior hippocampus was selective to individuals with high levels of HPA activity, and decreased activity in the motor cortex (M1) was selective to those with high levels of freezing behavior. Furthermore, activity in these phenotype-selective regions mediated relations between amygdala metabolism and different expressions of anxiety. These findings provide a framework for understanding the mechanisms that lead to heterogeneity in the clinical presentation of internalizing disorders and set the stage for developing improved interventions.

affective neuroscience | behavioral inhibition | developmental psychopathology | emotion | functional neuroimaging

There is substantial heterogeneity in the clinical presentation of anxiety disorders, both within and across diagnostic categories. Anxiety often emerges early in development and, here too, there is considerable variation in presentation. Clinically relevant anxiety is often accompanied and preceded by an anxious temperament (AT). AT is a trait-like phenotype that is evident early in life, stable over time, associated with increased amygdala reactivity to novelty and potential threat, and expressed similarly in children and young nonhuman primates (1–6). Extreme dispositional anxiety and behavioral inhibition in childhood is a well-established risk factor for the internalizing spectrum of psychiatric disorders, including anxiety and major depression (5, 7, 8). These disorders are highly prevalent and associated with substantial morbidity and mortality (9, 10). Like the internalizing disorders, childhood AT is a complex, multidimensional phenotype and children with extreme AT show varying mixtures of peripheral physiological, behavioral, and other kinds of anxiety-related symptoms (5, 11, 12). This diversity manifests as weak covariation among these features (2, 13, 14). From the perspective of diagnosis and treatment, an important unresolved question is the degree to which heterogeneity in anxious individuals' symptoms reflects fundamental differences or similarities in the underlying neurobiology. To address this question, we used a well-validated nonhuman primate model of early-life AT in combination with high-resolution ^{18}fluorodeoxyglucose (FDG)-positron emission tomography (FDG-PET) (2, 15).

Young rhesus macaques are ideal for understanding the neurobiology of dispositional anxiety in human children. Reflecting the two species recent evolutionary divergence, the brains of monkeys and humans are genetically, anatomically, and functionally similar (16–18). Homologous neurobiological substrates endow monkeys and humans with a shared repertoire of complex cognitive and socio-emotional behaviors (18). In particular, juvenile monkeys and young children express anxiety in similar ways, and in both species there are considerable individual differences in the presentation of the anxious phenotype. In monkeys, the AT phenotype can be elicited using the No-Eye Contact (NEC) condition of the Human Intruder Paradigm (15). During the NEC challenge, a human "intruder" enters the test room and presents his or her profile to the monkey while avoiding direct eye contact (15), similar to procedures used for assessing dispositional anxiety and behavioral inhibition in children (19). Using this challenge, individual differences in three fundamental dimensions of the anxious phenotype were assessed: hypothalamic-pituitary-adrenal (HPA) activity (increased plasma cortisol), behavior (increased freezing), and expressive communication (reductions in spontaneous vocalizations). All three dimensions show robust changes in response to the NEC challenge (15), paralleling observations made in dispositionally anxious and shy children (5).

A key advantage of the juvenile monkey AT model is that it permits concurrent measures of neural activity and naturalistic responses to an ethologically relevant potential threat, an opportunity not afforded by research in children. Here, FDG-PET was used to quantify brain metabolic activity in 238 freely behaving juvenile monkeys. FDG-PET, which provides a measure of regional brain metabolism integrated over the entire 30-min NEC challenge, is ideally suited for assessing sustained, trait-like neural responses (1).

Using these measures, we identified brain regions where metabolism predicts variation in one or more of the three AT dimensions. To understand the degree to which heterogeneity in the presentation of AT reflects invariant or distinct neural mechanisms, we distinguished "common" and "selective" substrates. Common neural substrates are those shared by individuals with varying expressions of anxiety; that is, a core set of brain regions where metabolism predicts variation in all three dimensions of the

Author contributions: A.S.F. and N.H.K. designed research; S.E.S. performed research; A.S.F. contributed new reagents/analytic tools; A.J.S., A.S.F., J.A.O., and N.H.K. analyzed data; and A.J.S., A.S.F., J.A.O., R.J.D., and N.H.K. wrote the paper.

The authors declare no conflict of interest.

This article is a PNAS Direct Submission.

[1]A.J.S. and A.S.F. contributed equally to this work.

[2]To whom correspondence should be addressed. E-mail: nkalin@wisc.edu.

This article contains supporting information online at www.pnas.org/lookup/suppl/doi:10.1073/pnas.1214364110/-/DCSupplemental.

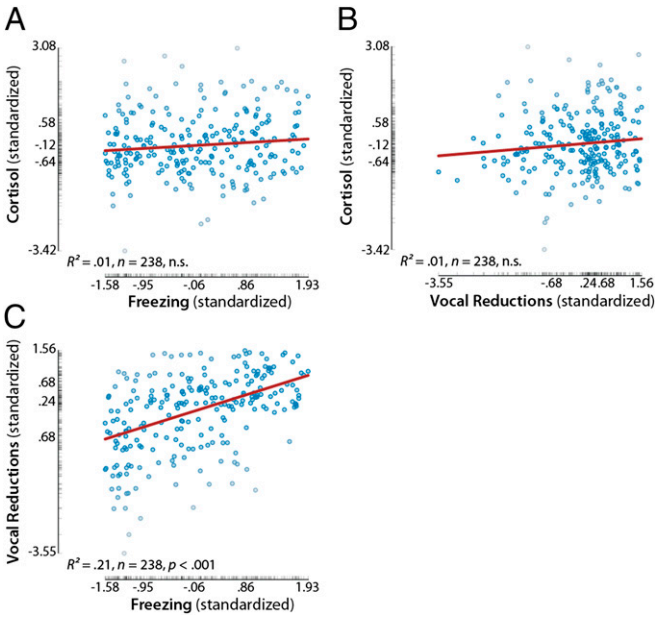

Fig. 1. Heterogeneity and continuity in the presentation of AT. Pairwise partial correlations revealed that cortisol was largely independent of freezing and vocal reductions (*A* and *B*). Freezing and vocal reductions were correlated but far from redundant (*C*). All three dimensions were continuously distributed, suggesting that AT represents a multidimensional spectrum of phenotypes, rather than a mixture of distinct subgroups. Axis labels indicate the minimum, maximum, and interquartile range.

AT phenotype (HPA activity, freezing behavior, and expressive communication). Based on imaging and lesion studies in monkeys and humans (4, 6, 20–22), we hypothesized that the central nucleus of the amygdala (Ce) would be among the regions identified as shared substrates. Selective neural substrates are those specifically engaged by individuals with high levels of a particular dimension; that is, regions where metabolism predicts variation in only one of the AT dimensions. Mechanistic studies in rodents suggest that the Ce can orchestrate a broad spectrum of responses to threat via projections to response-specific targets (23, 24). Therefore, we further hypothesized that the association between common substrates (e.g., Ce metabolism) and particular dimensions of the anxious phenotype would be mediated by the appropriate phenotype-selective substrate. Distinguishing common from selective substrates, and clarifying the nature of their relationships with one another, is important for understanding how phenotypic variation in AT early in development gives rise to heterogeneity in the clinical presentation of internalizing disorders later in life, for facilitating the development of improved therapeutic interventions, and for understanding emotional traits.

Results

Heterogeneity and Continuity in the Presentation of the AT Phenotype. Like other emotional traits, individual differences in the profile of anxiety-related symptoms manifests as weak covariation among anxiety-related measures (2, 13, 14). Consistent with this, in the present sample a series of robust regressions revealed that variation in cortisol was largely independent of freezing and vocal reductions, $R^2 < 0.02$, $P > 0.06$. As shown in Fig. 1, some individuals are characterized by extreme HPA activity and little freezing and vocal reductions, some show the opposite presentation, and yet others show intermediate presentations. Regression analyses also showed that, although individuals who froze more emitted fewer vocalizations, the two measures were far from redundant, $R^2 = 0.23$, $P < 0.001$. These results underscore the substantial heterogeneity in the presentation of AT. Furthermore, all three dimensions of the anxious phenotype were reliable (*SI Methods*) and continuously distributed (Fig. 1). This continuity suggests that AT, like the internalizing disorders (11, 12), represents a spectrum of closely related phenotypes rather than a mixture of categorically distinct subgroups.

Heterogeneity in the Phenotypic Presentation of AT Reflects both Common and Selective Substrates. Because HPA activity, freezing behavior, and vocal reductions are continuously distributed (Fig. 1), we adopted a dimensional approach to identifying the neural circuitry underlying different expressions of anxiety. Specifically, we performed a series of voxelwise partial correlations between metabolism and each AT dimension while accounting for variation in the other two (using robust regression techniques; see *SI Methods*). This process revealed a number of regions where metabolism predicted the unique variance in one or more dimensions of the phenotype, including the orbitofrontal cortex (OFC; areas 13 and 47), anterior insula (AI), primary motor cortex (M1), amygdala, hippocampus, and periaqueductal gray (PAG) (Fig. 2 and Tables S1–S3).

To distinguish common neural substrates, those shared by individuals with different expressions of the anxious phenotype, we used a three-way conjunction (i.e., logical AND) of the thresholded partial correlation maps shown in Fig. 2 to identify regions where metabolism predicted variation in HPA activity, freezing

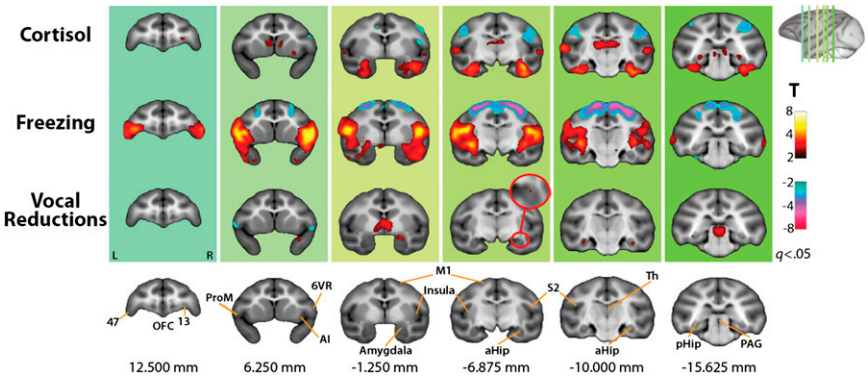

Fig. 2. Brain regions where metabolic activity significantly predicted one AT dimension independent of variation in the other two (FDR $q < 0.05$). Red circular inset shows magnified view. Coordinates indicate millimeter from the anterior commissure. aHip, anterior hippocampus; AI, anterior insula; L, left; M1, primary motor cortex (area 4); OFC, orbitofrontal cortex (architectonic areas 13 and 47); PAG, periaqueductal gray; pHip, posterior hippocampus; R, right; Th, thalamus.

behavior, and vocal reductions [false-discovery rate (FDR) $q < 0.05$]. As shown in Fig. 3, this analysis revealed a cluster in the right dorsal amygdala and bilateral clusters in the hippocampi (Table S4) (hemispheric asymmetry analyses were not significant for the amygdala cluster; see *SI Methods*). Using a probabilistic chemoarchitectonic map (*SI Methods*), we localized the dorsal amygdala cluster to the lateral division of the central nucleus (CeL) (Fig. S1). The magnitude of the three partial correlations was similar in the amygdala and anterior hippocampus ($P > 0.19$), reinforcing the idea that these regions make similar contributions to the three dimensions of the anxious phenotype. Taken together, these results demonstrate that elevated metabolism in the CeL and anterior hippocampus is a consistent feature of individuals with divergent phenotypic expressions of anxiety. This implication reflects the fact that the partial correlations estimate the unique relationship between each phenotype dimension and metabolism at a fixed level of the other two. For example, the partial correlation for cortisol indicates that individuals with high levels of HPA activity (and intermediate levels of freezing behavior and vocalizations on average) show more activity in the CeL and anterior hippocampus when compared with individuals with low levels of HPA activity (and intermediate levels of freezing behavior and vocalizations on average). For illustrative purposes, these effects are shown in Fig. S2. [Note: The results of the conjunction analysis suggest, but do not demonstrate, that aggregating the three dimensions—cortisol, freezing, and vocalization reductions—into a composite would provide a more sensitive index of AT-related variation in metabolic activity. Confirmatory analyses demonstrated that this was indeed the case (*SI Methods*).]

To distinguish selective neural substrates, regions that are specifically engaged by individuals with high levels of a particular AT dimension, we used a two-way conjunction to identify regions where metabolism: (*i*) predicted one of the three AT dimensions after controlling for variation in the other two (FDR $q < 0.05$) and (*ii*) explained more variance in that dimension compared with the other two (assessed using a voxelwise test of the difference in correlations; FDR $q < 0.05$). That is, we distinguished regions where one of the three partial correlations shown in Fig. 2 was both significant and significantly stronger than the other two. This process revealed a number of regions (Tables S1–S3). In particular, as shown in Fig. 4, individuals characterized by high levels of HPA activity were distinguished by elevated metabolic activity in the lateral anterior hippocampus, whereas those who presented with high levels of freezing behavior showed attenuated activity in the M1, and those with low levels of vocal communication showed increased activity in the ventrolateral prefrontal cortex (vlPFC). The lateral anterior hippocampal cluster that was selective to cortisol was located several millimeters from the nearest cluster that predicted all three AT dimensions (Fig. 3 and Table S4). These results clarify the neural systems underlying heterogeneity in the expression of anxiety.

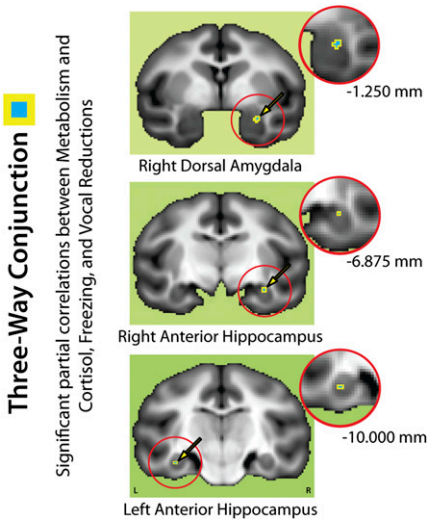

Fig. 3. Shared neural substrates: Amygdalar and hippocampal metabolism predicts all three dimensions of the AT phenotype. Figure depicts the three-way minimum conjunction (logical AND) of the significant partial correlations shown in Fig. 2. Regions shown in cyan/gold predicted the unique variance in all three dimensions of the AT phenotype. Circular insets show magnified views. For other conventions, see Fig. 2.

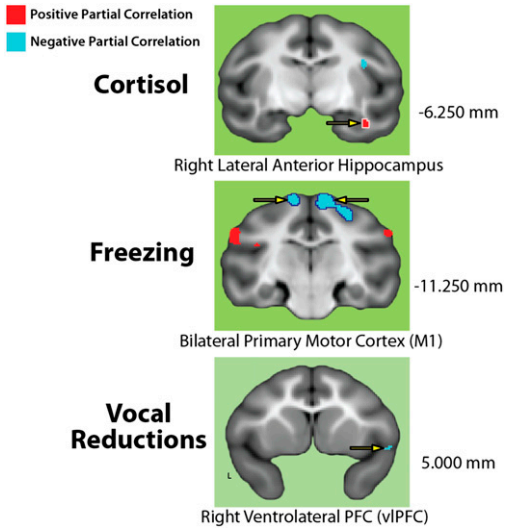

Fig. 4. Selective substrates: Regions where one AT dimension predicted significant variance in brain metabolism (partial correlation: FDR $q < 0.05$) and explained more variance than the other two dimensions (difference in correlations: FDR $q < 0.05$), identified using a two-way conjunction (logical AND). Conventions are described in Fig. 2.

We identified the CeL and anterior hippocampus as shared substrates, regions where metabolism predicts all three dimensions of the anxious phenotype. To assess whether those brain-phenotype relationships are explained by activity in phenotype-selective regions, we used a series of multivariate mediation models (*SI Methods*) to test whether the partial correlation between the shared substrates (Fig. 3) and a particular dimension of the AT phenotype depends on the relevant selective substrate (Fig. 4) (e.g., CeL → M1 → freezing). As shown in Fig. 5 and detailed in Table S5, this process demonstrated that relations between the shared substrates and HPA activity were mediated by activity in the cortisol-selective anterior hippocampal region, $P < 0.005$ (uncorrected). Similarly, relations between the shared substrates and freezing behavior were mediated by activity in M1, $P < 0.005$ (uncorrected). Significant mediation was not found for vocal reductions. To assess the specificity of the cortisol and freezing results, we recomputed the mediation models after reversing the candidate mediating regions (e.g., CeL → lateral anterior hippocampus → freezing). None of these control models was significant, indicating a double dissociation (Table S5). Specifically, metabolism in the lateral anterior hippocampus explains relations between the shared substrates and HPA activity, but not freezing behavior, whereas M1 metabolism explains relations between the shared substrates and freezing, but not HPA activity. Collectively, these results clarify how shared substrates can influence multiple dimensions of the anxious phenotype. In particular, these results indicate that relations between the core set of shared substrates, such as the CeL, and the endocrine and behavioral dimensions of the

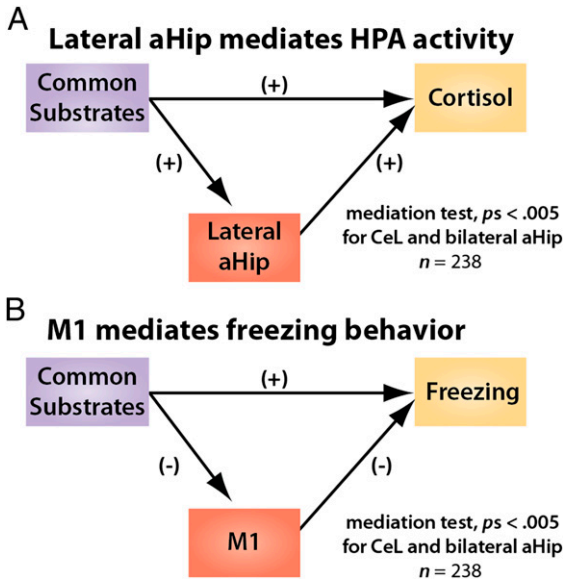

Fig. 5. Linking common and selective substrates: Brain-phenotype relations are selectively mediated. (*A*) Metabolism in the cortisol-selective region of lateral anterior hippocampus mediates relations between the common substrates (CeL and aHip) (Fig. 3) and HPA activity, $P < 0.005$ (uncorrected). (*B*) Metabolism in the freezing-selective region of M1 mediates relations between the common substrates and freezing behavior, $P < 0.005$ (uncorrected). The plus and minus symbols indicate the sign of the partial correlation (see Table S5).

anxious phenotype strongly depend upon regions that are dimension-specific.

Discussion

Like the internalizing disorders, there is marked variation in the presentation of AT during early development. Our observations provide compelling evidence that this heterogeneity reflects the joint contribution of common substrates, a core set of brain regions that are shared by individuals with different manifestations of extreme anxiety, and selective substrates, regions that are specifically associated with particular expressions. Consistent with prior work (2, 13, 14), the endocrine, behavioral, and communicative dimensions of the anxious phenotype were weakly correlated and continuously distributed, suggesting that AT represents a multidimensional spectrum of closely related phenotypes (Fig. 1). Using a dimensional analytic approach that circumvented the need to impose artificial categorical boundaries on the data, we identified a number of regions where metabolic activity predicts one or more dimensions of the AT phenotype (e.g., amygdala, hippocampus, PAG, AI, and OFC) (Fig. 2). We demonstrated that variation in each dimension of the phenotype—increased HPA activity, more freezing behavior, and fewer expressive vocalizations—was independently predicted by activity in the CeL and anterior hippocampus (Fig. 3). Elevated activity in this core set of brain regions was consistently found in individuals who displayed high levels of any of these dimensions (Fig. S2). We identified a second set of regions that specifically predict particular dimensions of the anxious phenotype, including the lateral anterior hippocampus and M1, and vlPFC (Fig. 4). Activity in these phenotype-selective regions distinguished individuals with high levels of HPA activity, freezing behavior, and vocal reductions, respectively. Finally, we demonstrated that these regions selectively mediate the association between the shared substrates, such as the CeL, and the endocrine and behavioral dimensions of the AT phenotype (Fig. 5). In sum, these observations suggest that variation in the expression of dispositional anxiety reflects the activity of a neurobiological system comprised of both shared and phenotype-selective components. As described below, these findings have mechanistic, translational, and theoretical implications.

With respect to mechanism, our results show that the CeL and anterior hippocampus are consistently engaged by individuals with divergent presentations of anxiety (Fig. 3 and Fig. S2). This finding is in accord with evidence that the amygdala and anterior hippocampus show exaggerated activation to potentially threat-relevant cues in individuals with a variety of anxiety disorders or a childhood history of extreme AT (6, 21). Similarly, lesions of either region attenuate many signs of anxiety (20, 22, 23, 25). Interestingly, recent work in rodents suggests that the CeL plays a key role in gating the output of the amygdala (26, 27). In particular, the CeL is poised to modulate both acute fear and sustained anxiety via inhibitory projections to the two major output stations of the extended amygdala: the medial division of the Ce and the lateral division of the bed nucleus of the stria terminalis (26, 27).

Our results indicate that individual differences in the expression of anxiety reflect the proximal contribution of phenotype-selective regions. In particular, we observed a double dissociation: M1 mediated freezing behavior, but not cortisol, whereas the lateral anterior hippocampus showed the opposite profile. The selective role of the lateral anterior hippocampus in the endocrine dimension of dispositional anxiety is consistent with mechanistic evidence that the hippocampus regulates the HPA axis (28). This result may reflect the dense distribution of mineralocorticoid receptors in the primate hippocampus (29), which are involved in more trait-like or basal aspects of HPA activity (28). The involvement of M1 in the behavioral dimension of AT is consistent with its well-established role in voluntary action. We obtained more limited evidence that the vlPFC is selectively involved in the reduction of expressive coo vocalizations, consistent with work implicating ventral premotor areas in vocalizations and other orofacial behaviors (30).

Although noninvasive techniques, such as FDG-PET, cannot establish causation, our results are in accord with mechanistic research demonstrating that the Ce orchestrates many of the peripheral physiological, behavioral, and expressive dimensions of anxiety and that these effects are mediated by functional interactions with response-specific targets (22–24). Our results address the proximal substrates of individual differences in the presentation of anxiety. Individuals characterized by high levels of freezing, for example, are distinguished by attenuated activity in M1. However, the distal determinants of this heterogeneity remain unclear; it may reflect variation in the strength of functional connectivity between the CeL and anterior hippocampus and particular phenotype-specific regions. Another possibility is that it reflects individual differences in subpopulations of phenotype-specific neurons that are intermingled at a level beyond the resolution of conventional imaging techniques (31). Indeed, evidence for distinct subpopulations of freezing- and cardiovascular-specific neurons in the Ce has led some investigators to suggest the possibility of developing therapeutic interventions targeting disorder-specific or patient-specific differences in symptom profiles (31), consistent with earlier suggestions in the translational literature (32).

Between one-third and two-thirds of anxiety patients are treatment-resistant or refractory (33), underscoring the need to develop more efficacious interventions. The present results highlight the potential utility of broad-spectrum (i.e., multisymptom) approaches. In particular, our findings suggest that therapeutics aimed at molecular targets within the CeL and anterior hippocampus, particularly when administered early in life, could ameliorate a variety of maladaptive or excessive responses to potential threat. Over time, such responses likely promote more complex and chronic symptoms (e.g., avoidance, anticipatory worry) and neurobiological alterations (34, 35). This suggestion is reinforced

by evidence that anxiety disorders with distinct presentations—including posttraumatic stress disorder, social anxiety disorder, specific phobias, and generalized anxiety disorder—are all characterized by elevated amygdala reactivity to aversive or potentially threatening stimuli (21, 36). Targeting upstream regions that are poised to regulate the CeL and anterior hippocampus (37), such as the OFC, represents another approach to broad-spectrum treatment. In this regard, cognitive-behavioral therapy, which is thought to be mediated by emotion regulatory processes implemented in the prefrontal cortex (38, 39), or cognitive-behavioral therapy combined with novel pharmacological interventions that increase neuroplasticity, may be particularly effective (40). Developing more effective early-life interventions is particularly important for minimizing the cumulative social and interpersonal damage associated with extreme anxiety and behavioral inhibition during early development (5).

These data also have implications for general theories of emotion. The peripheral physiological and behavioral features that are the hallmarks of emotion have traditionally been cast as tightly synchronized (41, 42). However, faced with growing evidence of weak response coupling, theorists have speculated that no single brain region could orchestrate all of these responses—that the alterations in the face, voice, body, and mental experience characteristic of emotional states and traits reflect the activity of segregated neural circuits (14, 43). This possibility is not addressed by prior imaging studies, which have typically measured only one or two concurrent responses or composite anxiety measures. Nor has it been directly addressed by lesion studies, which lack the statistical power required to investigate phenotypic heterogeneity. Therefore, the present observation that activity in the CeL and anterior hippocampus explains independent variation in endocrine, behavioral, and communicative responses to the NEC challenge provides unique grounds for rejecting strict claims of neural segregation. More generally, this finding indicates that a lack of strong covariation among different dimensions of anxiety does not preclude the existence of a response-independent substrate (44); individuals can vary in the strength and predominance of different anxiety dimensions, yet rely on the same core set of shared substrates.

In summary, using a well-validated nonhuman primate model of AT and high-resolution functional imaging, the present study demonstrates that striking diversity in the presentation of anxiety reflects the distinct contributions of both shared and phenotype-selective substrates. Individuals characterized by high levels of HPA activity, high levels of freezing behavior, or low levels of expressive vocalizations all exhibit elevated metabolic activity in the CeL and anterior hippocampus. These brain-phenotype associations were dependent upon a second set of regions, including the lateral anterior hippocampus and M1, which selectively mediate particular dimensions of the anxious phenotype. Importantly, these results were obtained using a relatively large unselected sample and robust analytic procedures, increasing the likelihood of replication. More broadly, these observations provide a framework for understanding the neurobiology of early-life anxiety and other emotional traits and set the stage for mechanistic studies aimed at identifying more effective interventions for the internalizing spectrum of disorders.

Methods

Subjects received FDG before testing. The AT phenotype was elicited by the presentation of a human intruder's profile (30-min). An observer quantified freezing behavior and expressive vocalizations. Following testing, plasma was collected and subjects were scanned. Higher FDG-PET signals indicate greater metabolism during testing. Plasma cortisol was quantitated by radioimmunoassay. MRI and PET images were processed using standard methods and normalized to a stereotactic template (0.625 mm^3). Robust regressions identified regions where activity predicted the unique variance in cortisol, freezing, and vocal reductions. Analyses controlled for nuisance variation in mean-centered age, sex, and voxelwise gray matter probability. Common and phenotype-selective substrates were identified using criteria described in the text. Mediation analyses used standard analytic techniques.

ACKNOWLEDGMENTS. We thank E. Ahlers, A. Alexander, V. Balchen, R. Birn, B. Christian, A. Converse, L. Friedman, M. Jesson, E. Larson, K. Mayer, T. Oakes, P. Roseboom, N. Vack, H. Van Valkenberg, L. Williams, the staffs of the Harlow Center for Biological Psychology, HealthEmotions Research Institute, and Wisconsin National Primate Center, and two anonymous reviewers for their assistance. This work was supported by the National Institutes of Health (NIH) (Grants HD003352, HD008352, MH018931, MH046729, MH081884, MH084051, MH091550, OD011106, and RR000167), the HealthEmotions Research Institute, and Meriter Hospital.

1. Fox AS, et al. (2012) Central amygdala nucleus (Ce) gene expression linked to increased trait-like Ce metabolism and anxious temperament in young primates. *Proc Natl Acad Sci USA* 109(44):18108–18113.
2. Fox AS, Shelton SE, Oakes TR, Davidson RJ, Kalin NH (2008) Trait-like brain activity during adolescence predicts anxious temperament in primates. *PLoS ONE* 3(7):e2570.
3. Kalin NH, Shelton SE, Takahashi LK (1991) Defensive behaviors in infant rhesus monkeys: Ontogeny and context-dependent selective expression. *Child Dev* 62(5): 1175–1183.
4. Oler JA, et al. (2010) Amygdalar and hippocampal substrates of anxious temperament differ in their heritability. *Nature* 466(7308):864–868.
5. Fox NA, Henderson HA, Marshall PJ, Nichols KE, Ghera MM (2005) Behavioral inhibition: Linking biology and behavior within a developmental framework. *Annu Rev Psychol* 56:235–262.
6. Blackford JU, Pine DS (2012) Neural substrates of childhood anxiety disorders: A review of neuroimaging findings. *Child Adolesc Psychiatr Clin N Am* 21(3):501–525.
7. Essex MJ, Klein MH, Slattery MJ, Goldsmith HH, Kalin NH (2010) Early risk factors and developmental pathways to chronic high inhibition and social anxiety disorder in adolescence. *Am J Psychiatry* 167(1):40–46.
8. Clauss JA, Blackford JU (2012) Behavioral inhibition and risk for developing social anxiety disorder: A meta-analytic study. *J Am Acad Child Adolesc Psychiatry* 51(10): 1066–1075.e1.
9. Kessler RC, Petukhova M, Sampson NA, Zaslavsky AM, Wittchen HU (2012) Twelve-month and lifetime prevalence and lifetime morbid risk of anxiety and mood disorders in the United States. *Int J Methods Psychiatr Res* 21(3):169–184.
10. Collins PY, et al.; Scientific Advisory Board and the Executive Committee of the Grand Challenges on Global Mental Health (2011) Grand challenges in global mental health. *Nature* 475(7354):27–30.
11. Rutter M (2011) Research review: Child psychiatric diagnosis and classification: Concepts, findings, challenges and potential. *J Child Psychol Psychiatry* 52(6):647–660.
12. Hyman SE (2010) The diagnosis of mental disorders: The problem of reification. *Annu Rev Clin Psychol* 6:155–179.
13. Buss KA, Davidson RJ, Kalin NH, Goldsmith HH (2004) Context-specific freezing and associated physiological reactivity as a dysregulated fear response. *Dev Psychol* 40(4): 583–594.
14. Barrett LF, Ochsner KN, Gross JJ (2007) On the automaticity of emotion. *Social Psychology and the Unconscious: The Automaticity of Higher Mental Processes*, ed Bargh J (Psychology Press, NY), pp 173–217.
15. Kalin NH, Shelton SE (1989) Defensive behaviors in infant rhesus monkeys: Environmental cues and neurochemical regulation. *Science* 243(4899):1718–1721.
16. Freese JL, Amaral DG (2009) Neuroanatomy of the primate amygdala. *The Human Amygdala*, eds Whalen PJ, Phelps EA (Guilford, NY), pp 3–42.
17. Gibbs RA, et al.; Rhesus Macaque Genome Sequencing and Analysis Consortium (2007) Evolutionary and biomedical insights from the rhesus macaque genome. *Science* 316(5822):222–234.
18. Preuss TM (2007) Primate brain evolution in phylogenetic context. *Evolution of Nervous Sytems*, eds Kaas JH, Preuss TM (Elsevier, NY), Vol 4, pp 3–34.
19. Kagan J, Reznick JS, Snidman N (1988) Biological bases of childhood shyness. *Science* 240(4849):167–171.
20. Feinstein JS, Adolphs R, Damasio A, Tranel D (2011) The human amygdala and the induction and experience of fear. *Curr Biol* 21:1–5.
21. Etkin A, Wager TD (2007) Functional neuroimaging of anxiety: A meta-analysis of emotional processing in PTSD, social anxiety disorder, and specific phobia. *Am J Psychiatry* 164(10):1476–1488.
22. Kalin NH, Shelton SE, Davidson RJ (2004) The role of the central nucleus of the amygdala in mediating fear and anxiety in the primate. *J Neurosci* 24(24):5506–5515.
23. Rodrigues SM, LeDoux JE, Sapolsky RM (2009) The influence of stress hormones on fear circuitry. *Annu Rev Neurosci* 32:289–313.
24. LeDoux JE, Iwata J, Cicchetti P, Reis DJ (1988) Different projections of the central amygdaloid nucleus mediate autonomic and behavioral correlates of conditioned fear. *J Neurosci* 8(7):2517–2529.
25. Sierra-Mercado D, Padilla-Coreano N, Quirk GJ (2011) Dissociable roles of prelimbic and infralimbic cortices, ventral hippocampus, and basolateral amygdala in the expression and extinction of conditioned fear. *Neuropsychopharmacology* 36(2): 529–538.

26. Ehrlich I, et al. (2009) Amygdala inhibitory circuits and the control of fear memory. *Neuron* 62(6):757–771.
27. Pare D, Duvarci S (2012) Amygdala microcircuits mediating fear expression and extinction. *Curr Opin Neurobiol* 22(4):717–723.
28. Jacobson L, Sapolsky R (1991) The role of the hippocampus in feedback regulation of the hypothalamic-pituitary-adrenocortical axis. *Endocr Rev* 12(2):118–134.
29. Sánchez MM, Young LJ, Plotsky PM, Insel TR (2000) Distribution of corticosteroid receptors in the rhesus brain: Relative absence of glucocorticoid receptors in the hippocampal formation. *J Neurosci* 20(12):4657–4668.
30. Coudé G, et al. (2011) Neurons controlling voluntary vocalization in the macaque ventral premotor cortex. *PLoS ONE* 6(11):e26822.
31. Viviani D, et al. (2011) Oxytocin selectively gates fear responses through distinct outputs from the central amygdala. *Science* 333(6038):104–107.
32. Davidson RJ (1978) Specificity and patterning in biobehavioral systems. Implications for behavior change. *Am Psychol* 33(5):430–436.
33. Bystritsky A (2006) Treatment-resistant anxiety disorders. *Mol Psychiatry* 11(9): 805–814.
34. Oler JA, et al. (2009) Serotonin transporter availability in the amygdala and bed nucleus of the stria terminalis predicts anxious temperament and brain glucose metabolic activity. *J Neurosci* 29(32):9961–9966.
35. Etkin A, Prater KE, Schatzberg AF, Menon V, Greicius MD (2009) Disrupted amygdalar subregion functional connectivity and evidence of a compensatory network in generalized anxiety disorder. *Arch Gen Psychiatry* 66(12):1361–1372.
36. Shin LM, Liberzon I (2010) The neurocircuitry of fear, stress, and anxiety disorders. *Neuropsychopharmacology* 35(1):169–191.
37. Fox AS, et al. (2010) Orbitofrontal cortex lesions alter anxiety-related activity in the primate bed nucleus of stria terminalis. *J Neurosci* 30(20):7023–7027.
38. DeRubeis RJ, Siegle GJ, Hollon SD (2008) Cognitive therapy versus medication for depression: Treatment outcomes and neural mechanisms. *Nat Rev Neurosci* 9(10):788–796.
39. Diekhof EK, Geier K, Falkai P, Gruber O (2011) Fear is only as deep as the mind allows: A coordinate-based meta-analysis of neuroimaging studies on the regulation of negative affect. *Neuroimage* 58(1):275–285.
40. Krystal JH, et al. (2009) Neuroplasticity as a target for the pharmacotherapy of anxiety disorders, mood disorders, and schizophrenia. *Drug Discov Today* 14(13–14):690–697.
41. Darwin C (2009) *The Expression of the Emotions in Man and Animals* (Oxford Univ Press, NY), 4th Ed.
42. Ekman P (1992) An argument for basic emotions. *Cogn Emotion* 6(3–4):169–200.
43. Barrett LF (2006) Are emotions natural kinds? *Perspect Psychol Sci* 1:28–58.
44. Mauss IB, Levenson RW, McCarter L, Wilhelm FH, Gross JJ (2005) The tie that binds? Coherence among emotion experience, behavior, and physiology. *Emotion* 5(2): 175–190.

Supporting Information

Shackman et al. 10.1073/pnas.1214364110

SI Methods

Hypothesis testing used the sample described in ref. 1, which focused on the heritability of metabolic activity in the medial temporal lobe. Methods for the elicitation and assessment of anxious temperament (AT) and the quantification of ^{18}fluorodeoxyglucose (FDG)-positron emission tomography (PET) are detailed in refs 1 and 2 and summarized here.

Subjects. Briefly, 240 prepubescent monkeys [*Macaca mulatta*; mean (SD) age = 2.41 (0.92) years; 51.3% female] from the Harlow Primate Laboratory or Wisconsin National Primate Research Center underwent behavioral testing and FDG-PET as part of a larger investigation of the genetic underpinnings of AT (1, 3). PET data from two individuals proved unusable. Housing and experimental procedures were performed in accord with guidelines set forth by the University of Wisconsin–Madison Institutional Animal Care and Use Committee.

Overview. Subjects received intravenous FDG immediately before the 30-min No-Eye Contact (NEC) challenge. Individual differences in behavioral responses (freezing and vocalizations) were quantified by an experienced observer. Following testing, plasma was collected for quantifying cortisol and subjects were deeply anesthetized (15 mg/kg ketamine), intubated, and positioned in a stereotactic device within the PET scanner. Metabolic activity during the PET scan reflects the amount of FDG uptake during the preceding behavioral paradigm; regions that were more metabolically active during the NEC challenge took up more radio-labeled glucose. Anesthesia was maintained using 1–2% (vol/vol) isoflurane gas. MRI were collected during a separate session. The median (SD) time between the FDG-PET and MRI sessions was 37.0 (37.5) d.

NEC Challenge. Individual differences in the three dimensions of the AT phenotype were elicited using the NEC component of the Human Intruder Paradigm (HIP) (4). The HIP is among the most commonly used procedures for measuring dispositional anxiety in nonhuman primates (5). Subjects were placed in a testing cage. Similar to laboratory procedures used for assessing AT in children (e.g., stranger approach) (6–8), potential threat took the form of a male human experimenter ("intruder") who entered the room and stood motionless ~2.5 m while presenting his profile to the subject (30 min).

Quantifying Individual Differences in the Three Dimensions of the AT Phenotype. NEC-elicited behavior was unobtrusively quantified by a well-trained rater using a closed-circuit audiovisual system. Freezing was defined as a period of >3 s characterized by a tense body posture and the absence of vocalizations or movements other than slow head movements or eye-blinks. "Coo" calls are contact or separation vocalizations that are elicited by exposure to the test cage (i.e., the "alone" condition of the HIP) and suppressed by exposure to the NEC challenge (i.e., human intruder's profile) (9–11). Coo vocalizations were defined as audible calls characterized by an increase then decrease in frequency and intensity made by rounding and pursing the lips. Mean freezing duration and cooing frequency were $\log_e$ and square-root transformed, respectively. Plasma cortisol (μg/dL) was quantified in duplicate using the DPC Coat-a-count radioimmunoassay (Siemens). Assaying procedures were highly reliable (interassay CV = 6.6%; intra-assay CV = 4.0%) and sensitive (lower detection limit = 1 μg/dL). Standardized cortisol, freezing, and vocalization responses were created (1, 2) by linearly removing nuisance variance in age and, for cortisol, time-of-day using SPSS (v20.0.0; IBM). Prior work indicates that cortisol, freezing, and coo vocalizations consistently show robust changes in response to the NEC challenge (4, 5, 11–23). Brain-behavior analyses used reverse-scored vocalizations ("vocal reduction" = $-1 \times$ coo-frequency$^{1/2}$) to ensure that effects were consistently signed across the three dimensions of the phenotype (i.e., higher values indicate more intense reactions to the phenotype-eliciting NEC challenge).

FDG-PET and MRI. FDG and attenuation scans were acquired using a Siemens/Concorde microPET P4 scanner (24). Images were reconstructed using standard filtered-backprojection techniques with attenuation- and scatter-correction. MRI were collected under anesthesia (see above) using a General Electric Discovery 3T scanner (GE) and standard quadrature extremity coil. Scans used a 3D T1-weighted inversion-recovery fast gradient echo prescription (TR/TE/Flip/ NEX /FOV/Matrix: 9.4 ms/2.1 ms/10°/2/ 140 mm/512 × 512; 248 × 1-mm axial slices; gap: −0.05 mm).

Processing Pipeline for Imaging Data. Before spatial normalization, brains were manually extracted from T1 images using SPAMALIZE (http://psyphz.psych.wisc.edu/~oakes/spam/spam_frames.htm). Brain-extracted T1 images were linearly registered (12 *df*) to a preexisting in-house macaque template (2) in the stereotactic space of Paxinos et al. (25) using FLIRT (http://fsl.fmrib.ox.ac.uk/fsl/flirt). Images were inspected and averaged to create an age-appropriate, study-specific linear template (0.625 mm × 0.625 mm × 0.625 mm = 0.244 mm^3). Native-space, brain-extracted T1 images were then nonlinearly registered to the template using FNIRT (http://www.fmrib.ox.ac.uk/fsl/fnirt). Normalized brains were segmented into gray matter (GM), white matter, and cerebrospinal fluid probability maps using FAST (www.fmrib.ox.ac.uk/fsl/fast4). Single-subject PET images were linearly registered to the corresponding native-space T1 images (6 *df*). The resulting transformation matrices were concatenated with those defining the nonlinear transformation to the study-specific standard template and then used to normalize the PET images. Normalized and interpolated PET images (0.625 mm × 0.625 mm × 0.625 mm = 0.244 mm^3) were global-mean scaled within the brain using SPAMALIZE. Scaled PET and GM probability maps were spatially smoothed (4-mm FWHM Gaussian). Some figures were created using MRIcron (http://www.mccauslandcenter.sc.edu/mricro/mricron).

Hypothesis Testing Strategy. The central aim of the present study was to distinguish common and selective neural substrates. Accordingly, we first identified regions where metabolic activity predicted variance in each of the three dimensions of the AT phenotype (cortisol, freezing, and vocal reduction) while controlling for the other two. Specifically, a series of whole-brain robust regression analyses were performed using MULTISTATIC (26), an extension of FMRISTAT (http://www.math.mcgill.ca/keith/fmristat). Consistent with recent recommendations (27, 28), analyses used robust procedures, which minimize the influence of outlying observations. Similar to other toolboxes for imaging data (29), robust regression in MULTISTATIC is implemented using the *robustfit* function in MATLAB (http://www.mathworks.com). In each analysis, one of the dimensions served as the explanatory variable and the other two served as covariates of no interest. Analyses also controlled for nuisance variation in mean-centered age, sex, and voxelwise GM probability, an indirect measure of differences in spatial normalization and gross anatomy (26). This

analytic procedure is formally equivalent to computing three voxelwise partial correlation maps.

Common substrates. Common neural substrates are those shared by individuals with varying expressions of extreme AT, a core set of brain regions where metabolism predicts variation in all three AT dimensions (cortisol levels, freezing behavior, and vocal reductions). To identify regions where individual differences in regional brain metabolism significantly predicted all three AT dimensions, the three partial correlation maps were thresholded using the false-discovery rate (FDR $q = 0.05$; whole-brain corrected across maps) (30, 31) and then combined using a three-way minimum conjunction test (i.e., logical AND) (32). The conjunction test yielded a "*t*-minimum" map containing voxels that were significant in all three parent maps; voxels satisfying this criterion were assigned the value corresponding to the *t*-statistic from the least-significant parent map, otherwise set to 0 (www.math.mcgill.ca/keith/fmristat/#conjunctions).

Selective substrates. Selective neural substrates are those specifically engaged by individuals with high levels of a particular dimension of the AT phenotype (e.g., freezing), regions where metabolism significantly and strongly predicts variation in only one of the AT dimensions. Selective regions were defined as those that: (*i*) were significantly correlated with one of the three dimensions of the AT phenotype (cortisol levels, freezing behavior, or vocal reductions; FDR $q < 0.05$), and (*ii*) explained significantly more variance in that dimension compared with the other two (FDR $q < 0.05$). Effectively, this process identified partial correlations that were both significant and significantly different from the other two (e.g., individual differences in freezing explained more variance in brain metabolic activity than cortisol and vocal reductions). Differences in correlations correlations were assessed using the Hotelling–Williams test (33, 34).

Mediation analyses. We identified the lateral division of the central nucleus of the amygdale (CeL) and anterior hippocampus as common substrates, regions where metabolism predicts each one of three dimensions constituting the AT phenotype (Fig. 3 and Table S4). To assess whether those brain-phenotype relationships are explained by activity in regions identified as selective, we used a series of multivariate mediation models to test whether the partial correlation between the common substrates and a particular dimension of the phenotype depends on the relevant selective substrate (e.g., CeL → M1 → freezing) (Fig. 4 and Tables S1–S3). We used a standard ordinary least squares (OLS) multivariate analytic framework (35, 36) (for recent applications to neuroimaging data, see refs. 37 and 38). Fully satisfying the criteria of this framework would demonstrate that a significant proportion of the association (i.e., partial correlation) between metabolic activity in one of the three common regions (e.g., CeL) and a particular AT dimension (e.g., freezing behavior) is predicted by metabolism in one of the candidate mediating region (e.g., M1, or the primary motor cortex). Operationally, this framework required four significant tests: (*i*) a common substrate predicts a particular dimension of AT, (*ii*) a selective substrate predicts a particular dimension of AT, (*iii*) the common substrate predicts the selective substrate, and (*iv*) controlling for variance in the selective substrate weakens the partial correlation between the common substrate and the relevant dimension of the AT phenotype. Consistent with our prior work (39), the final criterion was assessed using Clogg's test (35, 40). This test was conservatively thresholded at a nominal $P < 0.0057$ (Sidak-corrected for the nine tests-of-interest, one-tailed given the directional hypothesis). Because FDG-PET lacks the temporal resolution necessary to determine whether activity within the common substrates (e.g., CeL) temporally precedes differences in activity within the selective substrates (e.g., M1), this test does not provide evidence of causal mediation.

To assess the specificity of the mediation findings, we computed two kinds of control models (Table S5). For the first model, we recomputed each mediation model using another candidate mediator region as a control (e.g., using the cortisol-selective region for the freezing mediation model: CeL → lateral anterior hippocampus → freezing). For the second model, we recomputed each model using another AT dimension as a control (e.g., cortisol for the mediation model incorporating the freezing-selective region: CeL → M1 → cortisol). Control analyses were only computed for regions where significant mediation effects were obtained.

Phenotype Reliability Analyses. We computed test-retest reliability of individual differences in cortisol, freezing behavior, and vocal reductions for a subset of individuals exposed to the NEC challenge on three occasions over 1.21 y (SD = 0.27; $n = 63$). The first assessment occurred at the time of FDG-PET session featured in the main text. The rank-order of individual differences in cortisol, freezing, and vocal reduction were reliable over the three occasions (intraclass correlation = 0.66–0.88; mean single-response correlation between adjacent sessions = 0.46–0.79). These levels are similar to those obtained for self-report measures of affective traits (e.g., negative affect) in human adults over comparable spans (41). The true psychometric reliability of these measures (i.e., in the absence of genuine change) is likely to be somewhat higher because of the lengthy period from the first to the third sessions (42) and the fact that data were acquired during the peri-adolescent period, a period of substantial neural and psychological maturation (43). The composite index of AT (2) was also reliable (intraclass correlation = 0.83; mean correlation between adjacent sessions = 0.71).

Hemispheric Asymmetry Analyses for the Right Dorsal Amygdala. To test whether the right dorsal amygdala cluster identified by the three-way voxelwise conjunction (see Fig. 3 and Table S4) showed a significant hemispheric asymmetry, we computed the difference in correlations separately for each dimension of the AT phenotype. Regressions were conducted in SPSS using data extracted from the right dorsal amygdala cluster and the homologous region in the left hemisphere, and controlling for nuisance variance in mean-centered age, sex, and GM probability. Because none of the tests approached significance, $t < 1.46$, $P > 0.14$ (uncorrected), we refrain from interpreting the apparent laterality of this effect.

Probabilistic Chemoarchitectonic Map of the CeL. The amygdala is a complex structure, comprised of numerous anatomically and physiologically distinct nuclei (44). Here we used previously published in vivo serotonin transporter (5-HTT) binding data (45, 46) to localize the dorsal amygdala cluster to the CeL of the amygdala. Ex vivo research demonstrates that the lateral division of the primate central nucleus of the amygdala (CeL) expresses much higher 5-HTT levels compared with neighboring regions (47–50). Capitalizing on this chemoarchitectonic signature, we used the distribution of ^{11}C-DASB (a high-affinity radiolabeled 5-HTT ligand) from an independent sample of young monkeys to define a probabilistic CeL region of interest (Fig. S1). For detailed methods, see ref. 45; for a similar mapping application, see ref. 51. Briefly, 5-HTT availability was assayed using ^{11}C-DASB, a radiolabeled high-affinity 5-HTT ligand. Dynamic PET time series were transformed into voxelwise distribution volume ratio [DVR; an index of binding (52)] maps normalized to activity in a cerebellar reference region. Single-subject DVR maps were normalized to the study-specific template and averaged. The resulting probabilistic (i.e., mean) 5-HTT binding map was thresholded (250× cerebellum). We then assessed the degree of overlap with the conjunction-defined cluster. This process revealed that the peak amygdala voxel and most of the dorsal amygdala cluster overlapped with the ROI (Sørensen-Dice similarity coefficient = 0.86), indicating that individuals with different presentations of extreme AT commonly engage the CeL (Fig. S1).

AT Composite Is a More Sensitive Index of Metabolic Activity than any One of Its Constituents. The results of the conjunction analysis suggest, but do not demonstrate, that aggregating the three dimensions—cortisol, freezing, and reduced vocalizations—into a composite would provide a more sensitive index of AT-related variation in core network activity. Confirmatory analyses demonstrated that this was the case. Confirmatory analyses used techniques similar to those described in *Hypothesis Testing Strategy* (see above), but did not partial covariation across the three dimensions. This process revealed that the AT composite, computed as the arithmetic mean of the three standardized dimensions (2), explained significantly more variance in CeL and anterior hippocampal metabolic activity than any one of the constituent dimensions in the clusters identified by the voxelwise three-way conjunction analysis, $t > 2.18$, $P < 0.03$. Furthermore, planned contrasts revealed that the slope of the robust regression line fit to neural activity was significantly steeper for the AT composite compared with its constituents ($P < 0.04$, one-tailed). This finding indicates that individuals with a strong average response to the NEC—high levels of cortisol, long bouts of freezing, and few vocalizations—tended to show the highest levels of activity in the CeL and anterior hippocampus; conversely, individuals with a weak average response tended to show the lowest activity. Whole-brain analyses yielded similar conclusions.

These results also provide unique empirical support for the use of composite measures of AT and other dimensions of temperament. Often, such composites are derived using statistical criteria that mandate strong covariation among constituents (e.g., factor analysis). Our results empirically demonstrate the utility of multidimensional composites constructed from anxiety-related measures that are theoretically or clinically related, but not necessarily significantly intercorrelated. In fact, our composite AT index showed strong predictive validity despite showing relatively weak covariation among its constituent dimensions, consistent with empirical work by Kagan et al. and others (7, 53–55).

1. Oler JA, et al. (2010) Amygdalar and hippocampal substrates of anxious temperament differ in their heritability. *Nature* 466(7308):864–868.
2. Fox AS, Shelton SE, Oakes TR, Davidson RJ, Kalin NH (2008) Trait-like brain activity during adolescence predicts anxious temperament in primates. *PLoS ONE* 3(7):e2570.
3. Rogers J, Shelton SE, Shelledy W, Garcia R, Kalin NH (2008) Genetic influences on behavioral inhibition and anxiety in juvenile rhesus macaques. *Genes Brain Behav* 7(4):463–469.
4. Kalin NH, Shelton SE (1989) Defensive behaviors in infant rhesus monkeys: Environmental cues and neurochemical regulation. *Science* 243(4899):1718–1721.
5. Corcoran CA, et al. (2012) Long-term effects of differential early rearing in rhesus macaques: Behavioral reactivity in adulthood. *Dev Psychobiol* 54(5):546–555.
6. Volbrecht MM, Goldsmith HH (2010) Early temperamental and family predictors of shyness and anxiety. *Dev Psychol* 46(5):1192–1205.
7. Kagan J, Reznick JS, Snidman N (1988) Biological bases of childhood shyness. *Science* 240(4849):167–171.
8. Hirshfeld-Becker DR, et al. (2008) Behavioral inhibition. *Depress Anxiety* 25(4): 357–367.
9. Fox AS, et al. (2005) Calling for help is independently modulated by brain systems underlying goal-directed behavior and threat perception. *Proc Natl Acad Sci USA* 102(11):4176–4179.
10. Bauers KA, de Waal FBM (1991) "Coo" vocalizations in stumptailed macaques: A controlled functional analysis. *Behaviour* 119(1–2):143–160.
11. Kalin NH, Shelton SE (1998) Ontogeny and stability of separation and threat-induced defensive behaviors in rhesus monkeys during the first year of life. *Am J Primatol* 44(2):125–135.
12. Kalin NH, Shelton SE, Davidson RJ, Kelley AE (2001) The primate amygdala mediates acute fear but not the behavioral and physiological components of anxious temperament. *J Neurosci* 21(6):2067–2074.
13. Izquierdo A, Murray EA (2004) Combined unilateral lesions of the amygdala and orbital prefrontal cortex impair affective processing in rhesus monkeys. *J Neurophysiol* 91(5): 2023–2039.
14. Izquierdo A, Suda RK, Murray EA (2005) Comparison of the effects of bilateral orbital prefrontal cortex lesions and amygdala lesions on emotional responses in rhesus monkeys. *J Neurosci* 25(37):8534–8542.
15. Machado CJ, Bachevalier J (2008) Behavioral and hormonal reactivity to threat: Effects of selective amygdala, hippocampal or orbital frontal lesions in monkeys. *Psychoneuroendocrinology* 33(7):926–941.
16. Golub MS, Hogrefe CE, Widaman KF, Capitanio JP (2009) Iron deficiency anemia and affective response in rhesus monkey infants. *Dev Psychobiol* 51(1):47–59.
17. Friedman EM, Reyes TM, Coe CL (1996) Context-dependent behavioral effects of interleukin-1 in the rhesus monkey (*Macaca mulatta*). *Psychoneuroendocrinology* 21(5):455–468.
18. Kalin NH, Shelton SE, Turner JG (1991) Effects of alprazolam on fear-related behavioral, hormonal, and catecholamine responses in infant rhesus monkeys. *Life Sci* 49(26):2031–2044.
19. Kalin NH, Shelton SE, Takahashi LK (1991) Defensive behaviors in infant rhesus monkeys: Ontogeny and context-dependent selective expression. *Child Dev* 62(5): 1175–1183.
20. Kalin NH, Shelton SE, Rickman M, Davidson RJ (1998) Individual differences in freezing and cortisol in infant and mother rhesus monkeys. *Behav Neurosci* 112(1):251–254.
21. Kalin NH, Larson C, Shelton SE, Davidson RJ (1998) Asymmetric frontal brain activity, cortisol, and behavior associated with fearful temperament in rhesus monkeys. *Behav Neurosci* 112(2):286–292.
22. Kalin NH, Shelton SE, Fox AS, Oakes TR, Davidson RJ (2005) Brain regions associated with the expression and contextual regulation of anxiety in primates. *Biol Psychiatry* 58(10):796–804.
23. Coleman K, Dahl RE, Ryan ND, Cameron JL (2003) Growth hormone response to growth hormone-releasing hormone and clonidine in young monkeys: Correlation with behavioral characteristics. *J Child Adolesc Psychopharmacol* 13(3):227–241.
24. Tai C, et al. (2001) Performance evaluation of the microPET P4: A PET system dedicated to animal imaging. *Phys Med Biol* 46(7):1845–1862.
25. Paxinos G, Huang X, Petrides M, Toga A (2009) *The Rhesus Monkey Brain in Stereotaxic Coordinates* (Academic, San Diego), 2nd Ed.
26. Oakes TR, et al. (2007) Integrating VBM into the General Linear Model with voxelwise anatomical covariates. *Neuroimage* 34(2):500–508.
27. Poldrack RA (2012) The future of fMRI in cognitive neuroscience. *Neuroimage* 62(20): 1216–1220.
28. Schwarzkopf DS, De Haas B, Rees G (2012) Better ways to improve standards in brain-behavior correlation analysis. *Front Hum Neurosci* 6:200.
29. Wager TD, Keller MC, Lacey SC, Jonides J (2005) Increased sensitivity in neuroimaging analyses using robust regression. *Neuroimage* 26(1):99–113.
30. Genovese CR, Lazar NA, Nichols T (2002) Thresholding of statistical maps in functional neuroimaging using the false discovery rate. *Neuroimage* 15(4):870–878.
31. Nichols T (2007) False discovery rate procedures. *Statistical Parametric Mapping. The Analysis of Functional Brain Images*, eds Friston K, Ashburner J, Kiebel S, Nichols T, Penny W (Elsevier, NY), pp 246–252.
32. Nichols T, Brett M, Andersson J, Wager T, Poline JB (2005) Valid conjunction inference with the minimum statistic. *Neuroimage* 25(3):653–660.
33. Steiger JH (1980) Tests for comparing elements of a correlation matrix. *Psychol Bull* 87(2):245–251.
34. Williams EJ (1959) The comparison of regression variables. *J R Stat Soc, B* 21(2): 396–399.
35. MacKinnon DP, Lockwood CM, Hoffman JM, West SG, Sheets V (2002) A comparison of methods to test mediation and other intervening variable effects. *Psychol Methods* 7(1):83–104.
36. Baron RM, Kenny DA (1986) The moderator-mediator variable distinction in social psychological research: Conceptual, strategic, and statistical considerations. *J Pers Soc Psychol* 51(6):1173–1182.
37. Lim SL, Padmala S, Pessoa L (2009) Segregating the significant from the mundane on a moment-to-moment basis via direct and indirect amygdala contributions. *Proc Natl Acad Sci USA* 106(39):16841–16846.
38. Wager TD, Davidson ML, Hughes BL, Lindquist MA, Ochsner KN (2008) Prefrontal-subcortical pathways mediating successful emotion regulation. *Neuron* 59(6):1037–1050.
39. Shackman JE, Shackman AJ, Pollak SD (2007) Physical abuse amplifies attention to threat and increases anxiety in children. *Emotion* 7(4):838–852.
40. Clogg CC, Petkova E, Shihadeh ES (1992) Statistical methods for analyzing collapsibility in regression models. *J Educ Stat* 17(1):51–74.
41. Watson D, Walker LM (1996) The long-term stability and predictive validity of trait measures of affect. *J Pers Soc Psychol* 70(3):567–577.
42. Chmielewski M, Watson D (2009) What is being assessed and why it matters: The impact of transient error on trait research. *J Pers Soc Psychol* 97(1):186–202.
43. Kalin NH, Shelton S (2000) The regulation of defensive behaviors in rhesus monkeys. *Anxiety, Depression, and Emotion*, ed Davidson RJ (Oxford Univ Press, NY), pp 50–68.
44. Freese JL, Amaral DG (2009) Neuroanatomy of the primate amygdala. *The Human Amygdala*, eds Whalen PJ, Phelps EA (Guilford, NY), pp 3–42.
45. Christian BT, et al. (2009) Serotonin transporter binding and genotype in the nonhuman primate brain using [C-11]DASB PET. *Neuroimage* 47(4):1230–1236.
46. Oler JA, et al. (2012) Evidence for coordinated functional activity within the extended amygdala of non-human and human primates. *Neuroimage* 61(4):1059–1066.
47. O'Rourke H, Fudge JL (2006) Distribution of serotonin transporter labeled fibers in amygdaloid subregions: implications for mood disorders. *Biol Psychiatry* 60(5): 479–490. Available at www.sciencedirect.com/science/journal/00063223.
48. Freedman LJ, Shi C (2001) Monoaminergic innervation of the macaque extended amygdala. *Neuroscience* 104(4):1067–1084.
49. Bauman MD, Amaral DG (2005) The distribution of serotonergic fibers in the macaque monkey amygdala: An immunohistochemical study using antisera to 5-hydroxytryptamine. *Neuroscience* 136(1):193–203.

50. Yilmazer-Hanke DM (2012) Amygdala. *The Human Nervous System*, eds Mai JK, Paxinos G (Academic, San Diego), pp 759–834.
51. Oler JA, et al. (2009) Serotonin transporter availability in the amygdala and bed nucleus of the stria terminalis predicts anxious temperament and brain glucose metabolic activity. *J Neurosci* 29(32):9961–9966.
52. Innis RB, et al. (2007) Consensus nomenclature for in vivo imaging of reversibly binding radioligands. *J Cereb Blood Flow Metab* 27(9):1533–1539.
53. Kagan J, Snidman N, McManis M, Woodward S, Hardway C (2002) One measure, one meaning: multiple measures, clearer meaning. *Dev Psychopathol* 14(3):463–475.
54. Epstein S (1986) Does aggregation produce spuriously high estimates of behavior stability? *J Pers Soc Psychol* 50(6):1199–1210.
55. Rushton JP, Brainerd CJ, Pressley M (1983) Behavioral development and construct validity: The principle of aggregation. *Psychol Bull* 94(1):18–38.

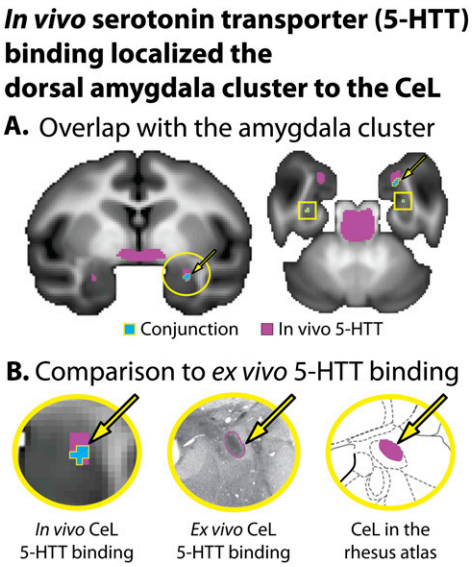

Fig. S1. In vivo serotonin transporter (5-HTT) binding localized the dorsal amygdala cluster to the CeL. High levels of 5-HTT binding are a hallmark of the lateral subdivision of the CeL. (*A*) Overlap between the amygdala cluster from the conjunction analysis (gold arrow; see Fig. 3) and in vivo 5-HTT availability (magenta). High 5-HTT availability was also observed along the midline (substantial innominata and raphe), but not in the anterior hippocampal clusters shown in the axial view (gold boxes). (*B*) Comparison with ex vivo 5-HTT binding. From left to right, magnified coronal views of the overlap shown in *A*, ex vivo 5-HTT binding, and the CeL in the rhesus atlas [adapted with permission from ref. 25, Copyright Elsevier (2009)]. The ex vivo image is a low-power photomicrograph of 5-HTT immunohistochemistry [adapted with permission from ref. 47, Copyright Elsevier (2006)].

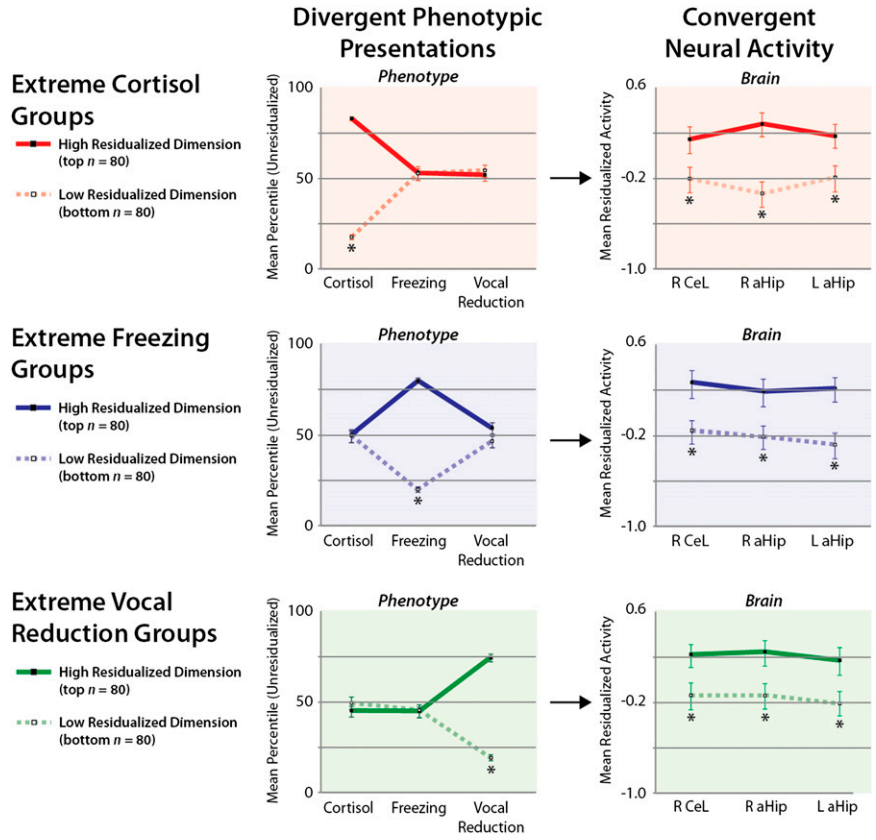

Fig. S2. Implications of the partial correlation analyses illustrated using a tercile split of the three residualized AT dimensions. The conjunction analysis demonstrates a consistent pattern of metabolic activity in the CeL and anterior hippocampus across divergent presentations of the AT phenotype. Divergent phenotypic presentations: To illustrate these effects, we plotted mean phenotype profiles for groups of individuals with high or low levels of each AT dimension. As with the partial correlation analyses, each dimension was residualized to remove variance predicted by the other two. A tercile split was used to identify extreme groups (n = 80 per group) separately for each residualized dimension (*Top* tercile: solid lines; *Bottom* tercile: broken lines). The panels on the left illustrate how this procedure sorts individuals into groups with divergent presentations of AT. Convergent neural activity: To illustrate the consistency of neural activity across divergent presentations, mean neural activity for the extreme groups (± SEM) is shown on the right. Individuals with high levels of cortisol, freezing, or vocal reductions (and intermediate levels of the other two responses on average) evinced greater activity compared with those with low levels. aHip, anterior hippocampus; CeL, lateral division of the central nucleus of the amygdala; L, left; R, right.

Table S1. Cluster descriptive statistics for regions where cerebral metabolism predicts cortisol

Sign of the partial correlation	Cluster	Cluster volume (mm^3)	Regions within the cluster	Millimeters from AC In template			Cortisol partial correlation t*	Cortisol vs. freezing $t^{\dagger}$	Cortisol vs. vocal reductions $t^{\dagger}$
				x	y	z			
Regions where cerebral metabolism significantly predicts cortisol after controlling for variation in freezing and vocal reductions[‡]									
Negative	Bi visual	3092.04	R V1	2.500	−44.375	1.250	−3.42	NA	NA
			R V2	−9.375	−36.250	10.000	−3.34	NA	NA
			R V2/V3V	15.000	−38.750	−8.750	−4.56	NA	NA
			R V2/V3D	15.625	−33.750	6.250	−3.22	NA	NA
			R V4V	21.250	−26.875	−8.125	−3.43	NA	NA
	L visual	0.49	V1	−15.625	−33.750	6.250	−2.81	NA	NA
	L visual	450.20	V1/V2	−15.625	−33.750	6.250	−2.81	NA	NA
			V3V	−8.125	−43.125	−8.750	−4.69	NA	NA
	L parietal	49.07	PE in the depths of IPS	−10.625	−21.250	13.750	−3.57	NA	NA
	L central	342.29	PE	−18.125	−15.625	16.875	−3.11	NA	NA
			Area 1	−21.250	−5.625	13.125	−3.87	NA	NA
			Area 2	−21.875	−9.375	11.875	−3.47	NA	NA
			Area 4 (F1)	−18.750	−4.375	11.875	−3.77	NA	NA
	R central	1352.05	PE	18.125	−12.500	15.625	−4.68	NA	NA
			Area 3A	18.750	−5.000	8.750	−4.15	NA	NA
			S2	20.625	−5.625	6.250	−4.06	NA	NA
			Area 2	21.250	−11.250	10.625	−3.93	NA	NA
			Area 4 (F1)	19.375	−3.750	16.875	−3.14	NA	NA
			Areas 44/6VR (F5) adjacent to IAR	21.250	4.375	9.375	−3.49	NA	NA
	L motor	1.46	Area 4 (F1)	−10.000	−12.500	21.875	−2.85	NA	NA
	L midcingulate	18.80	Areas p32′/24d′ in the fundus of CgS	−5.625	−2.500	13.750	−3.23	NA	NA
	R OFC	12.70	Areas 11/47	15.000	20.000	6.875	−3.38	NA	NA
Positive	R brainstem	0.73	Brainstem	1.875	−13.125	−10.000	2.81	NA	NA
	L midbrain	177.00	Colliculus	−3.125	−18.750	−2.500	4.12	NA	NA
			Isthmus of the cingulate	−3.125	−18.750	1.250	3.73	NA	NA
	R midbrain	71.53	Colliculus	3.750	−18.750	−3.125	3.77	NA	NA
	Bi thalamus	352.54	L dorsal thalamus	−5.000	−10.625	3.125	4.01	NA	NA
			R dorsal Thalamus	3.750	−8.750	5.000	3.77	NA	NA
	Bi striatum	343.02	L BNST	−2.500	2.500	−0.625	3.07	NA	NA
			L Caudate	−2.500	5.000	2.500	3.25	NA	NA
			L Lat septum	−1.875	3.750	2.500	3.24	NA	NA
			R Lat septum	1.250	3.125	0.625	3.16	NA	NA
			R Caudate	3.750	4.375	3.750	3.34	NA	NA
	L Ant hippocampus[‡]	1236.33	TF	−18.750	−11.250	−12.500	4.80	NA	NA
			Area 36 (TLR)	−16.250	−7.500	−15.000	4.58	NA	NA
			Ant hippocampus	−13.125	−3.750	−10.000	4.89	NA	NA
	R Ant hippocampus[§]	65.43	Caudal entorhinal	9.375	−2.500	−13.750	3.23	NA	NA
			Areas 35/36 (TLR)	19.375	−8.125	−15.000	5.50	NA	NA
			Ant hippocampus	−16.875	−6.250	−11.250	5.92	NA	NA
	L post hippocampus	51.27	Post hippocampus	−12.500	−17.500	−4.375	3.73	NA	NA
	R post hippocampus	65.43	Post hippocampus	12.500	−18.125	−3.750	3.75	NA	NA
	L Sup temporal	321.53	PaAL	−28.125	−10.000	1.875	4.76	NA	NA
	R Sup temporal	293.95	TPO	24.375	−11.250	0.000	4.15	NA	NA
			ST2	24.375	2.500	−4.375	3.87	NA	NA
			PaAL	28.750	−6.250	−1.875	3.39	NA	NA
	R claustrum	22.22	Claustrum	12.500	6.875	−3.125	3.24	NA	NA
	R OFC	7.57	Area 13L	12.500	11.875	3.750	3.21	NA	NA
Regions where cerebral metabolism significantly and selectively predicts cortisol									
Negative	R Lat visual	0.24	V2	16.875	−39.375	−8.750	−4.21	−3.02	−2.97
	L Lat visual	8.30	V4D/TEO	−21.250	−23.750	0.000	−3.03	−3.93	−3.58
	R Lat visual	90.58	V4V	20.625	−30.000	−3.125	−2.94	−3.09	−3.24
			V3	20.625	−30.000	1.250	−3.23	−4.06	−3.22
			V4D/TEO	22.500	−24.375	2.500	−3.28	−3.73	−3.76
	R parietal	0.24	Area PE in IPS	18.750	−13.75	15.000	−4.30	−2.97	−3.14
	R mid-insula	34.42	Gustatory Cortex and S2	18.125	−4.375	4.375	−3.41	−5.65	−3.12

Table S1. Cont.

Sign of the partial correlation	Cluster	Cluster volume (mm^3)	Regions within the cluster	Millimeters from AC In template			Cortisol partial correlation t*	Cortisol vs. freezing $t^{\dagger}$	Cortisol vs. vocal reductions $t^{\dagger}$
				x	y	z			
Positive	R cerebellum	38.33	Paraflocculus	−15.625	−16.875	−10.625	4.23	5.59	3.04
	L parahippocampus	0.24	PHG and isthmus of the cingulate	−10.625	−18.750	−4.375	2.96	4.83	2.97
	R parahippocampus	3.91	PHG and isthmus of the cingulate	12.500	−18.750	−4.375	3.56	2.99	3.02
	L Inf temporal	8.54	Area 36 (TH)	−18.750	−11.250	−12.500	4.79	2.97	4.14
	R Inf temporal	99.12	Area 36 (TH)	16.250	−9.375	−13.750	5.17	3.00	2.98
	L post cingulate	37.35	Area 23	−3.125	−18.750	1.250	3.73	3.20	3.08
	R hippocampus	6.84	Lat Ant hippocampus	16.875	−6.250	−11.250	5.92	3.49	3.29

AC, anterior commissure; Ant, anterior; Bi, bilateral; BNST, bed nucleus of the stria terminalis; CeL, lateral division of the central nucleus of the amygdala; CgS, cingulate sulcus; dlPFC, dorsolateral prefrontal cortex; IAR, inferior arcuate sulcus; Inf, inferior; IPS, intraparietal sulcus; L, left; Lat, lateral; NA, not applicable; OFC, orbitofrontal cortex; PHG, parahippocampal gyrus; Post, posterior; R, right; Sup, superior. White matter clusters are omitted. Regions were labeled using Paxinos et al. (25), freely available at http://scalablebrainatlas.incf.org/main/coronal3d.php?template=PHT00&.

*Robust regression controlling for variation in mean-centered age, sex, gray matter probability, standardized freezing duration, and standardized vocal reductions (whole-brain FDR $q < 0.05$).

†Williams T2 test for the difference in dependent correlations (whole-brain FDR $q < 0.05$).

‡Cluster contains the left anterior hippocampal cluster identified as a shared substrate (see Table S4).

§Cluster contains the right anterior hippocampal and dorsal amygdala (CeL) clusters identified as shared substrates (Table S4).

Table S2. Cluster descriptive statistics for regions where cerebral metabolism predicts freezing

Sign of the partial correlation	Cluster	Cluster volume (mm^3)	Freezing: Regions within the cluster	Millimeters from AC in template			Freezing partial correlation t*	Freezing vs. cortisol $t^{\dagger}$	Freezing vs. vocal reductions $t^{\dagger}$
				x	y	z			
Regions where cerebral metabolism significantly predicts freezing after controlling for variation in cortisol and vocal reductions									
Negative	Bi hemispheres	17882.32	L Ventral parafloccus	−15.625	−18.125	−11.250	−4.44	NA	NA
			R ventral parafloccus	15.000	−20.000	−10.625	−3.84	NA	NA
			R CB5 and ventral parafloccus	15.625	−26.250	−8.750	−5.16	NA	NA
			L CB5	−1.250	−23.750	−5.000	−4.70	NA	NA
			R CB5	2.500	−23.750	−3.750	−4.61	NA	NA
			L V2/V1	−9.375	−27.500	−2.500	−8.19	NA	NA
			R V1	10.625	−25.000	2.500	−6.20	NA	NA
			R V2	5.625	−30.625	0.000	−7.42	NA	NA
			R MST	13.125	−24.375	12.500	−4.84	NA	NA
			R MST and TPOC	15.000	−24.375	8.125	−5.68	NA	NA
			L PO and V3D in the fundus of POS	−6.875	−33.750	6.250	−4.49	NA	NA
			L V4	−18.125	−25.625	−7.500	−4.12	NA	NA
			L MSTV and MT (V5)	−15.000	−24.375	8.750	−4.56	NA	NA
			L PEC and PGM	−3.125	−31.250	13.750	−4.36	NA	NA
			L PE (MIP) in the depths of IPS	−10.625	−23.125	16.875	−7.98	NA	NA
			L PO (LIPE) in the depths of IPS	−9.375	−25.000	13.125	−5.02	NA	NA
			R PO (LIPE/LIPI) in the depths of IPS	6.875	−26.250	13.750	−5.07	NA	NA
			R areas 6/32′ (gyral) and 4 (F1)	0.000	−4.375	17.500	−4.08	NA	NA
			L dorsal area 4 (F1)	−6.250	−11.250	22.500	−6.39	NA	NA
			R dorsal area 4 (F1)	3.750	−11.875	21.875	−6.30	NA	NA
			R Lat area 4 (F1)	13.750	−8.750	17.500	−6.24	NA	NA
			L area 8D in the depths of SAR	−11.875	3.750	11.250	−3.79	NA	NA
			R area 8D in the depths of SAR	10.000	4.375	14.375	−3.70	NA	NA
			R area 6DR (F7)	10.625	8.125	16.875	−3.46	NA	NA
Positive	L Lat visual	1336.91	Lat V2	−28.125	−27.500	0.000	5.46	NA	NA
			TEO	−28.750	−20.625	0.625	4.74	NA	NA
			TEM and TE3	−28.750	−13.750	−1.875	3.57	NA	NA
	L midbrain	0.49	Midbrain	−2.500	−5.625	−6.250	2.80	NA	NA

Table S2. Cont.

Sign of the partial correlation	Cluster	Cluster volume (mm^3)	Freezing: Regions within the cluster	Millimeters from AC in template			Freezing partial correlation t*	Freezing vs. cortisol $t^{\dagger}$	Freezing vs. vocal reductions $t^{\dagger}$
				x	y	z			
	R midbrain	4.64	Reticular formation	5.625	−9.375	−6.250	2.88	NA	NA
	L hemisphere[‡]	6728.52	Lat nucl. of the amygdala	−13.125	1.875	−10.000	3.33	NA	NA
			Piriform and claustrum	−12.500	3.750	−6.250	3.57	NA	NA
			PFG and PFOp	−25.000	−11.875	10.625	4.24	NA	NA
			TE	−23.125	0.000	−14.375	3.20	NA	NA
			TPPro	−20.000	6.875	−9.375	4.12	NA	NA
			Area 38 (TLR)	−13.125	7.500	−15.625	3.33	NA	NA
			S2	−23.125	−3.750	3.125	6.86	NA	NA
			Gustatory cortex and AI	−19.375	6.250	1.250	5.84	NA	NA
			Area 4 (F1)	−27.500	−1.250	8.125	3.71	NA	NA
			Area 6VR (F5)	−23.125	7.500	6.250	5.04	NA	NA
			Area 47L	−23.125	13.125	−0.625	4.42	NA	NA
			Area 47O	−18.125	10.625	0.625	5.45	NA	NA
	R Hemisphere [§]	6176.03	Lat V2	26.250	−26.875	−1.875	5.16	NA	NA
			Ce and ventral putamen	13.125	−4.375	−6.875	4.37	NA	NA
			GI, ProKM, and Claustrum	18.125	−6.250	−3.750	4.87	NA	NA
			Area 2	24.375	−11.875	10.625	3.84	NA	NA
			TE3 and TEO	28.750	−17.500	−1.250	3.75	NA	NA
			TPO and TAa	22.500	0.625	−9.375	5.67	NA	NA
			Areas S2 and 2/1	23.750	3.125	−1.250	7.06	NA	NA
			Gustatory cortex	21.250	5.625	0.000	6.97	NA	NA
			Area 47	15.000	20.000	6.875	3.43	NA	NA
	L temporal	0.98	TE3	−26.250	−8.750	−11.250	2.83	NA	NA
	R temporal	3.91	TE3	25.625	−10.000	−12.500	3.05	NA	NA
	R temporal pole	66.16	Areas 36 (TLR) and TPPro	15.000	7.500	−16.875	3.43	NA	NA
	L vmPFC	197.51	Area 14M	−0.625	25.000	1.875	3.00	NA	NA
	R dlPFC	39.55	Area 8B	5.625	15.625	16.250	2.89	NA	NA
Regions where cerebral metabolism significantly and selectively predicts freezing									
Negative	Bi mesial visual and cerebellum	1284.18	L V2	−9.375	−27.500	−2.500	−8.19	−4.07	−4.77
			Bi CB4/5	−1.250	−23.750	−5.000	−4.70	−3.73	−3.32
			R V2	5.625	−30.625	0.000	−7.42	−2.96	−4.30
			R V1	10.625	−25.000	2.500	−6.20	−4.40	−5.13
			R SCL	15.625	−26.250	−8.750	−5.16	−3.03	−3.68
	R dorsal STS	0.98	MT (V5), MSTV, MSTD, and TPOC	15.625	−24.375	8.125	−5.66	−3.07	−2.95
	L motor	81.79	Dorsomesial area 4 (F1)	−6.250	−11.250	22.500	−6.39	−3.87	−5.66
	L motor	101.81	Lat area 4 (F1) adjacent to CS	−13.125	−6.875	19.375	−5.66	−4.48	−4.75
			Area 6DC (F2)	−12.500	1.250	18.125	−5.48	−4.48	−3.44
	R motor	280.52	Dorsomesial area 4 (F1)	3.750	−11.875	21.875	−6.30	−4.16	−6.36
			Area 4 (F1) along SPCD	9.375	−7.500	20.625	−6.24	−3.47	−5.25
			Lat area 4 (F1) adjacent to CS	13.750	−8.750	17.500	−6.24	−3.59	−5.19
	L FEF	24.17	Areas 6DR (F7) and 8AD/B in the fundus of SAR	−11.875	3.750	11.250	−3.79	−3.23	−3.83
	R FEF	0.24	Area 6DC (F2) in the posterior-dorsal bank of SAR	15.000	0.625	15.625	−4.14	−3.00	−3.01
Positive	L Lat visual	92.77	V1	−28.125	−27.500	0.000	5.46	4.79	3.49
	R Lat visual	118.90	V1	26.250	−26.875	−1.875	5.16	5.11	3.33
	L temporal	1.22	Area TEO	−28.750	−20.625	0.625	4.74	3.72	2.98
	R temporal	1.22	Area TPO	21.250	2.500	−9.375	5.22	2.96	4.12
	L insula/OFC	1891.60	Area PFx	−25.000	−11.875	10.625	4.24	4.72	3.66
			GI, claustrum, and putamen	−17.500	−6.875	−3.750	5.74	3.32	4.49

Table S2. Cont.

Sign of the partial correlation	Cluster	Cluster volume (mm^3)	Freezing: Regions within the cluster	Millimeters from AC in template			Freezing partial correlation t*	Freezing vs. cortisol $t^{\dagger}$	Freezing vs. vocal reductions $t^{\dagger}$
				x	y	z			
			S2	−24.375	2.500	1.875	6.59	5.53	5.68
			AI and S2	−19.375	6.250	1.250	5.84	4.69	4.81
			Dorsal Area 6VR (F5)	−23.125	7.500	6.250	5.04	4.89	4.23
			Areas 44, 47O, and ProM	−18.125	10.625	0.625	5.45	3.51	4.91
			Area 47L	−23.125	13.125	−0.625	4.42	4.45	4.32
	R insula/OFC	1492.43	Area PFx	24.375	−11.875	10.625	3.84	5.33	2.96
			GI, Claustrum, and Putamen	16.875	−9.375	−0.625	4.55	2.99	3.58
			S2	21.250	−4.375	3.125	6.54	6.91	5.11
			Ventral Area 2/1	23.750	3.125	−1.250	7.06	4.38	7.06
			Gustatory Cortex	21.250	5.625	0.000	6.97	4.77	6.46
			Area 47L	24.375	11.250	1.875	5.16	4.55	4.80
	L OFC	11.96	Area 47	−15.625	19.375	6.875	3.85	3.77	3.38
	R OFC	25.15	Area 47	15.000	20.000	6.875	3.43	4.93	3.51

AC, anterior commissure; AI, anterior insula; Bi, bilateral; CeL, lateral division of the central nucleus of the amygdala; CS, central sulcus; dlPFC, dorsolateral prefrontal cortex; FEF, frontal eye field; GI, granular insula; IAR, inferior arcuate sulcus; IPS, intraparietal cortex; L, left; Lat, lateral; NA, not applicable; Nucl, nucleus; OFC, orbitofrontal cortex; POS, parieto-occipital sulcus; R, right; SAR, superior arcuate sulcus; SCL, simple cerebellar lobule; SPSD, superior precentral dimple; STS, superior temporal sulcus; vmPFC, ventromedial prefrontal cortex. White matter clusters are omitted. Regions were labeled using Paxinos et al. (25), freely available at http://scalablebrainatlas.incf.org/main/coronal3d.php?template=PHT00&.

*Robust regression controlling for variation in mean-centered age, sex, gray matter probability, standardized plasma cortisol, and standardized vocal reductions (whole-brain FDR $q < 0.05$).

[†]Williams T2 test for the difference in dependent correlations (whole-brain FDR $q < 0.05$).

[‡]Cluster contains the left anterior hippocampal cluster identified as a shared substrate(see Table S4).

[§]Cluster contains the right anterior hippocampal and dorsal amygdala (CeL) clusters identified as shared substrates (see Table S4).

Table S3. Cluster descriptive statistics for regions where cerebral metabolism predicts vocal reductions

Sign of the partial correlation	Cluster	Cluster volume (mm^3)	Vocal reductions: Regions within the cluster	mm from AC in template			Vocal reductions partial correlation t*	Vocal reductions vs. cortisol $t^{\dagger}$	Vocal reductions vs. freezing $t^{\dagger}$
				x	y	z			
Regions where cerebral metabolism significantly predicts vocal reductions after controlling for variation in cortisol and freezing									
Negative	R visual	2.44	V2	6.875	−21.875	−2.500	−2.90	NA	NA
	Bi visual	480.47	L V2	−7.500	−21.250	−1.875	−3.79	NA	NA
			L PGM	−2.500	−33.750	3.125	−2.97	NA	NA
			R PGM	1.875	−28.125	5.000	−3.15	NA	NA
			L area 23 and PGM	−1.875	−22.500	5.000	−4.42	NA	NA
	R dorsal parietal	494.63	DP	10.000	−31.875	17.500	−4.34	NA	NA
	R Lat parietal	31.49	PG	20.000	−23.750	11.250	−3.50	NA	NA
	L OFC/vlPFC	39.55	ProM	−25.000	6.250	−0.625	−3.30	NA	NA
	R OFC/vlPFC	83.25	ProM	23.750	8.750	−2.500	−3.86	NA	NA
Positive	R PAG	181.88	PAG	0.625	−15.625	−2.500	3.79	NA	NA
	Bi thalamus	594.24	L dorsal thalamus	−1.250	−3.750	4.375	4.21	NA	NA
			R dorsal thalamus	0.625	−3.750	4.375	4.18	NA	NA
			L ventral Ant thalamus	3.125	−3.125	0.000	4.50	NA	NA
	L hippocampus[‡]	63.23	Ant hippocampus	−15.625	−11.875	−7.500	3.42	NA	NA
	R hippocampus[§]	34.67	Ant hippocampus	16.250	−11.250	−10.000	3.48	NA	NA
	R amygdala[¶]	137.45	Ce	10.625	−1.250	−8.125	3.36	NA	NA
Regions where cerebral metabolism significantly and selectively predicts Vocal reductions									
Negative	R Parietal	0.24	DP	10.625	−33.125	17.500	−4.01	−3.07	−2.95
	R vlPFC	5.62	ProM and ST2	23.125	5.000	−3.125	−3.15	−3.63	−6.91

AC, anterior commissure; Ant, anterior; Bi, bilateral; Ce, central nucleus of the amygdala; CeL, lateral division of the central nucleus of the amygdala; Lat, lateral; L:,left; OFC, orbitofrontal cortex; PAG, periaqueductal gray; R, right; vlPFC, ventrolateral prefrontal cortex. White matter clusters are omitted. Regions were labeled using Paxinos et al. (25), freely available at http://scalablebrainatlas.incf.org/main/coronal3d.php?template=PHT00&.

*Robust regression controlling for variation in mean-centered age, sex, gray matter probability, standardized cortisol, and standardized freezing duration (whole-brain FDR $q < 0.05$).

[†]Williams T2 test for the difference in dependent correlations (whole-brain FDR $q = 0.05$).

[‡]Cluster contains the left anterior hippocampal cluster identified as a shared substrate (Table S4).

[§]Cluster contains the right anterior hippocampal cluster identified as a shared substrate (Table S4).

[¶]Cluster contains the right dorsal amygdala (CeL) cluster identified as a shared substrate (Table S4).

Table S4. Cluster descriptive statistics for regions where cerebral metabolism predicts the unique variance in standardized plasma cortisol levels, freezing, and vocal reductions

Cluster	Cluster volume (mm^3)	Millimeters from AC in template			Three-way conjunction of partial correlations*
		x	*y*	*z*	Robust minimum $t^{\dagger}$
R dorsal amygdala[‡]	4.394	11.875	−1.250	−9.375	2.96
R anterior hippocampus	0.244	14.375	−6.875	−9.375	2.81
L anterior hippocampus	0.732	−15.625	−10.000	−9.375	2.87

*Robust regression controlling for variation in mean-centered age, sex, and voxelwise GM probability.
[†]Minimum across the three thresholded partial correlation maps (whole-brain FDR $q < 0.05$).
[‡]As detailed in *SI Methods*, hemispheric asymmetry analyses for the right dorsal amygdala cluster were not significant.

Table S5. Descriptive statistics for cluster mediation analyses

Candidate mediating region[‡]	AT dimension	Common substrates[¶]	Mediation test		Effect sizes for mediation paths (regressions)			Specificity analyses							
								Control mediating region				Control AT dimension			
					Common substrate → AT dimension	Common substrate → Candidate mediator	Candidate mediator → AT dimension	M1*		Lat Ant hippo[†]		Freezing		Cortisol	
			Tt	*P*[§]	*t*[‖]	*t*[‖]	*t*[‖]	*t*[**]	*P*[§]	*t*[**]	*P*[§]	*t*[††]	*P*[§]	*t*[††]	*P*[§]
Lat Ant hippo[†]	Cortisol	L Ant hippo	4.09	<0.005	3.09	11.00	5.40	−0.05	NS	—	—	−0.86	NS	—	—
		R Ant hippo	2.99	<0.005	4.53	16.40	5.40	−0.46	NS	—	—	−1.57	NS	—	—
		R CeL	4.36	<0.005	3.07	8.69	5.40	−0.15	NS	—	—	−0.56	NS	—	—
M1*	Freezing	L Ant hippo	5.19	<0.005	2.55	−4.41	−5.54	—	—	−0.86	NS	—	—	−0.05	NS
		R Ant hippo	5.00	<0.005	3.01	−4.21	−5.54	—	—	−1.57	NS	—	—	−0.46	NS
		R CeL	4.73	<0.005	3.25	−4.60	−5.54	—	—	−0.56	NS	—	—	−0.15	NS
vlPFC[‡‡]	Vocal reductions	L Ant hippo	−3.63	NS[¶¶]	2.79	1.03	−3.13	—	—	—	—	—	—	—	—
		R Ant hippo	−3.17	NS[¶¶]	2.55	2.08	−3.13	—	—	—	—	—	—	—	—
		R CeL	−3.95	NS[¶¶]	2.89	3.83	−3.13	—	—	—	—	—	—	—	—

Ant, anterior; AT, anxious temperament; CeL, the lateral division of the central nucleus of the amygdala; Hippo, hippocampus; L, left hemisphere; Lat, lateral; M1, primary motor cortex (area 4); NS, nonsignificant ($P > 0.05$, one-tailed, Sidak-corrected for nine tests); R, right hemisphere; vlPFC, ventrolateral prefrontal cortex. Regions were labeled using Paxinos et al. (25), freely available at http://scalablebrainatlas.incf.org/main/coronal3d.php?template=PHT00&.
*The dorsomesial motor region (area 4) that was selective to freezing (Table S2).
[†]The lateral anterior hippocampal region that was selective to cortisol (Table S1).
[‡]Hypothesis testing focused on whether selective regions mediated the association between each of the three core (common) regions and the three dimensions of the AT phenotype.
[¶]The three regions detailed in Table S4.
[§]Uncorrected *P*.
[‖]OLS regression controlling for variation in mean-centered age, sex, GM probability, and the two nontarget AT dimensions (i.e., a partial correlation analysis). Significant results for the corresponding whole-brain robust regressions (FDR $q < 0.05$) are detailed in Tables S1–S4.
**T-statistic for the mediation test using a control region (e.g., testing whether the lateral anterior hippocampal region that was selective to cortisol mediates the association between CeL and freezing).
[††]T-statistic for the mediation test using a control dimension of AT (e.g., testing whether M1 mediates the association between Ce and cortisol).
[‡‡]The vlPFC region that was selective to vocal reductions (Table S3).
[¶¶]This region displayed a suppressive relationship; the amount of variance in vocal reductions that was predicted by each one of the shared substrates was increased rather than decreased after accounting for the influence of the candidate mediator (vlPFC).